Vol. 740: 43–60, 2024
https://doi.org/10.3354/meps14636

MARINE ECOLOGY PROGRESS SERIES
Mar Ecol Prog Ser

Published July 25

Vertical distribution of Pacific oyster *Crassostrea gigas* larvae and modeling larval transport in Hiroshima Bay, Japan

Goh Onitsuka[1,*], Katsuyuki Abo[1], Tadashi Matsubara[1], Ken-ichiro Mizuno[2], Shun-ichiro Ikeda[3,6], Takafumi Sato[3,7], Tomoyuki Shikata[4], Toshimitsu Onduka[1], Masami Hamaguchi[5]

[1]Hatsukaichi Field Station, Fisheries Technology Institute, Japan Fisheries Research and Education Agency, Hatsukaichi, Hiroshima 739-0452, Japan

[2]Fisheries and Marine Technology Center, Hiroshima Prefectural Technology Research Institute, Kure, Hiroshima 737-1207, Japan

[3]Hiroshima City Fisheries Promotion Center, Nishi-ku, Hiroshima 733-0833, Japan

[4]Goto Field Station, Fisheries Technology Institute, Japan Fisheries Research and Education Agency, Goto, Nagasaki 853-0508, Japan

[5]Faculty of Marine Science and Technology, Fukui Prefectural University, Obama, Fukui 917-0116, Japan

[6]*Present address:* Environmental Conservation Division Noise and Air Pollution Section, Environment Bureau, the City of Hiroshima, Naka-ku, Hiroshima 730-8586, Japan

[7]*Present address:* Fisheries Division, Agriculture, Forestry, and Fisheries Department, Economic Affairs and Tourism Bureau, the City of Hiroshima, Naka-ku, Hiroshima 730-8586, Japan

ABSTRACT: Understanding vertical distribution of planktonic larvae is essential for elucidating larval dispersal and recruitment processes. We investigated the vertical distribution and horizontal transport of Pacific oyster *Crassostrea gigas* larvae by field observations and numerical simulations during their main spawning season in Hiroshima Bay, Japan. In field observations, despite horizontal differences and slight diurnal/semi-diurnal changes depending on larval sizes, most larvae were distributed in the upper 3 m layer. The relationship between *C. gigas* larvae and environmental conditions revealed that larval density increased with increasing temperature and chlorophyll *a* concentration, and the density peaked at salinity of approximately 20 for all larval sizes. The observed results suggest that the distribution characteristics of *C. gigas* larvae are suitable for survival in an estuarine area, where environmental conditions are potentially favorable but hydrodynamic conditions can drastically change over the short term due to variations in river discharge. To examine the effect of high river discharge on larval transport, numerical simulations were conducted using a particle-tracking model incorporating the vertical motion of *C. gigas* larvae. The simulation results reproduced the spatio-temporal dynamics of planktonic and settled larvae after the high river discharge. Although most particles simulating larvae outflowed from the main spawning area, an area of high particle density at the end of simulation corresponded with the offshore area for seedling collection. The present study suggests the role of vertical distribution of *C. gigas* larvae for recruitment, and the prospect of sustainability in oyster aquaculture with respect to seedling collection despite the frequent heavy rainfall associated with climate change.

KEY WORDS: Oyster larvae · Vertical distribution · Spatio-temporal dynamics · Particle-tracking model · River discharge · Settlement · Seedling collection

1. INTRODUCTION

Almost all commercially important bivalves have a planktonic larval stage in their early life cycle. Given the weak swimming ability of larvae compared with horizontal current velocities, the spatio-temporal dynamics of larvae are strongly affected by background ocean currents. In coastal areas, which are

*Corresponding author: onitsuka_go81@fra.go.jp

their main habitat, complex flow fields are induced by topography and various external forces such as tides, winds, and freshwater inputs from rivers. When conditions are stratified, in particular, vertical differences in flow structures have a large impact on horizontal larval transport through species specific and/or ontogenetic vertical distributions of larvae, which are key to dispersal and recruitment (North et al. 2008, Puckett et al. 2014, Peteiro & Shanks 2015, McVeigh et al. 2017).

The Pacific oyster *Crassostrea gigas* (Thunberg, 1793), one of the most important cultured bivalve species, is farmed in many coastal areas around the world (https://www.fao.org/fishery/docs/DOCUMENT/aquaculture/CulturedSpecies/file/en/en_pacificcuppedoyster.htm). Japan, *C. gigas*' native habitat, is one of the world's leading oyster-producing countries, and Hiroshima Bay is the largest *C. gigas* farming area in Japan. In Hiroshima Bay, almost all spat required for oyster farming are obtained by natural seedling collection, which is achieved by installing spat collectors made of scallop *Mizuhopecten yessoensis* shells during the *C. gigas* spawning season (Arakawa 1990, Matsubara et al. 2023). Although natural seedling collection is an important process indispensable for sustainable aquaculture of Pacific oyster, failure of seedling collection often occurs in the bay. Several studies have reported possible causes for failure of seedling collection from physical and biological aspects such as larval outflow from farming areas by horizontal advection (Kimura et al. 1975), harmful algae (Mizuno et al. 2015), the effects of chemicals such as antifouling biocides (Onduka et al. 2022), and feeding conditions (Wahyudin & Yamamoto 2020, Matsubara et al. 2023).

The planktonic larval period of *C. gigas*, from spawned eggs to settlement in substrate, lasts approximately 2 wk (Fujiya 1970, Koganezawa 1978, Arakawa 1990, Vogeler et al. 2016). In Hiroshima Bay, *C. gigas* spawning mainly occurs in summer, from July to August (Arakawa 1990). The first half of the main spawning period coincides with the rainy and post rainy season in western Japan. The rainy season associated with the East Asian summer monsoon is a typical meteorological event that supplies high precipitation in early summer (Ding & Chan 2005). In coastal areas, the rainy season causes drastic changes in water quality and hydrodynamic conditions in the surface layer within a daily time scale because of intermittent heavy discharge from rivers. Thus, the vertical distribution of *C. gigas* larvae is likely to largely affect their spatial distribution especially in this season; for a better understanding of the spatio-temporal dynamics of larvae and optimal seedling collection location, knowing the vertical distribution of larvae and the factors controlling their vertical position is critical.

Several studies have investigated the vertical distribution of *C. gigas* larvae (Kikuchi 1960, Arakawa 1990, Sugawara et al. 2000). In field observations, Kikuchi (1960) and Sugawara et al. (2000) reported the vertical distribution of *C. gigas* larvae according to size classes. Their results showed that most larvae were distributed from the surface to 2–6 m depth. Kikuchi (1960) also suggested the effect of ontogenetic and environmental changes on the vertical distribution of larvae. However, the relationship between vertical distribution and environmental conditions remains unclear. In addition, this lack of biological characterisation of vertical motion makes it difficult to conduct numerical modeling studies on larval transport of *C. gigas* (Kakehi 2022). The application of numerical models to this species is limited to either experiments with various assumptions of vertical behavior (Robins et al. 2017) or calculations that incorporate the biological characteristics of other oyster species (Kakehi et al. 2020). As for other oyster species, there are numerical studies on vertical swimming behavior and horizontal larval transport based on experimental and observational results (e.g. Dekshenieks et al. 1996, North et al. 2008). North et al. (2008) developed a larval transport model incorporating the vertical motions of 2 species, those of *C. virginica* and *C. ariakensis*. Their results reproduced differences in dispersion distance dependent on species-specific swimming behavior.

In the present study, we first conducted field observations in Hiroshima Bay during and after the rainy season to elucidate the vertical distribution of *C. gigas* larvae and the relationship with environmental conditions. Second, we conducted larval transport simulations using a particle-tracking model incorporating the vertical motions of larvae to examine the spatio-temporal dynamics of larvae before and after high river discharge. Finally, based on both observations and simulations, we discuss the role of vertical distribution of *C. gigas* larvae for recruitment, and the prospect of sustainability in oyster aquaculture with respect to seedling collection.

2. MATERIALS AND METHODS

2.1. Study area

Hiroshima Bay is a semi-enclosed embayment located in the western part of the Seto Inland Sea, Japan

(Fig. 1). The bay is sheltered by several islands and the mean depth is approximately 26 m (Kamiyama et al. 2005, Umehara et al. 2018). The bay is one of the most intensive oyster farming areas in Japan. The main farming area is northern Hiroshima Bay, including Etajima Bay, which connects with an offshore area through the Ohno, Nasabi, and Kure Straits. Water properties are mostly affected by the discharge of freshwater and nutrients, mainly from the Ohta River (Kamiyama et al. 2005, Umehara et al. 2018, Abo & Onitsuka 2019, Yamamoto et al. 2021). In fact, estuary circulation is driven by the fresh water discharged from the Ohta River in summer (Lee et al. 2001, Yamamoto et al. 2011, Abo & Onitsuka 2019).

2.2. Cross-sectional observations

To examine vertical distributions of *C. gigas* larvae and the relationship with environmental conditions, cross-sectional observations were conducted using the RV Shirafuji-maru along a transect line running from north to south of Hiroshima Bay at Stations (Stns) 1–6 during about 3 h around noon on 7, 16, 21, and 28 July 2020, respectively (Fig. 1). Water samples were pumped using a submersible pumping gear attached with a weighted flexible hose at depths of 1, 2, 3, 5, 7, and 10 m. *C. gigas* larvae were collected by filtering 250 l of seawater through a 50 µm mesh net. These samples were concentrated and immediately frozen at −20°C. In the laboratory, *C. gigas* larvae were identified using specific fluorescent-labeled monoclonal antibodies, and a light microscope was used to count them and measure their shell heights (Kakehi et al. 2020). To determine if there were ontogenetic changes in larval behavior, we divided them into 3 size classes: small (⩽150 µm, D-shaped larvae and small umbo), medium (150–210 µm, medium umbo), and large (>210 µm, large umbo and pediveliger). The proportion of each size class of larvae found at each depth was calculated using all larval profiles.

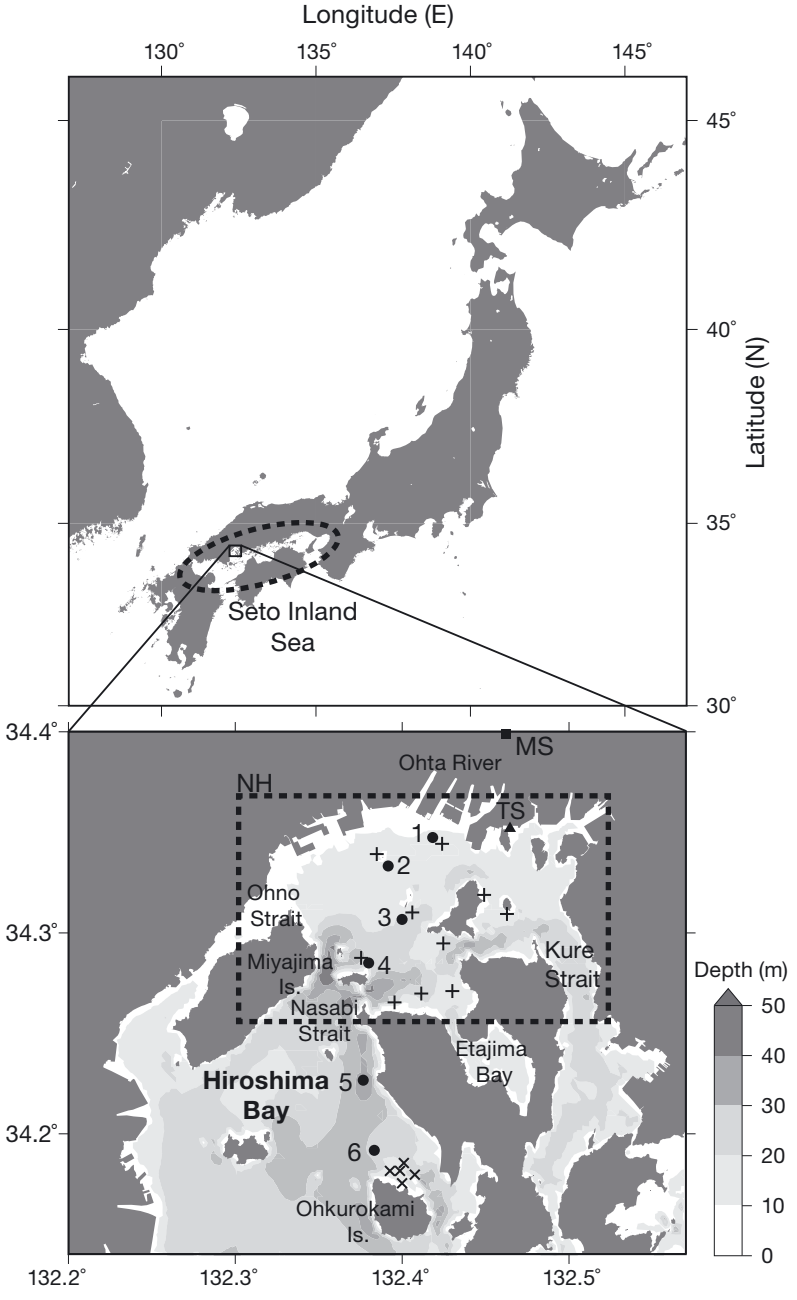

Fig. 1. Study area in Hiroshima Bay, Japan. Closed circles indicate the observation stations (Stns 1–6). Closed square and triangle indicate the meteorological (MS) and tidal station (TS), respectively. Plus and cross symbols indicate the monitoring stations of the Hiroshima City Fisheries Promotion Center in the northern area (northern Hiroshima Bay) and in the offshore area (near Ohkurokami Island), respectively. NH (dashed rectangle) indicates the initial particle position for Lagrangian particle-tracking simulations

Vertical profiles of water temperature, salinity, and chlorophyll fluorescence were measured at 0.1 m intervals at each station using a multi-parameter water quality sensor (AAQ-RINKO, JFE Advantech). Water samples pumped from depths of 1 or 3 m were

used for analyzing chlorophyll *a* (chl *a*) concentrations. One liter of seawater was filtered through Whatman GF/F filters, and the pigments were extracted by *N*,*N*-dimethylformamide. The *in vivo* chlorophyll fluorescence observed by AAQ-RINKO was calibrated using the chl *a* values determined by a fluorometer (10-AU, Turner Designs) in the laboratory. Coefficients of determination R^2 for linear regressions ranged from 0.975 to 0.997 in 4 cross-sectional observations. To examine the relationship between larval density and environmental factors, Spearman's rank correlations were calculated between logarithmic larval density collected at depths of 1, 2, 3, 5, 7, and 10 m and water temperature, salinity and chl *a* concentration observed at the same depths from the vertical profiles measured at 0.1 intervals. In addition, the relationship between logarithmic larval density and salinity was approximated by using a quadratic function.

2.3. 24 h stationary fixed-point observation

To examine the diurnal changes in larval vertical distributions, stationary fixed-point observation was conducted every 3 h for 24 h beginning at 08:00 Japan Standard Time (JST) on 3 August 2017 at Stn 3 (Fig. 1; ca. 23 m depth), which is located at the center of northern Hiroshima Bay. The RV Shirafuji-maru provided a platform to deploy the instruments. The methods of sampling, identifying, and counting *C. gigas* larvae were the same as for cross-sectional observations. Water samples were pumped using submersible pumping gear attached with a weighted flexible hose at 7–10 layers with 1–5 m intervals from 1 m depth to 1 m above the bottom. Water samples at the sea surface were collected using a plastic bucket. Considering that the abundances of medium- and large-sized larvae were 2 or 3 orders of magnitude smaller than small-sized larvae, the sum of medium- and large-sized larvae (i.e. medium–large size) was used for visualization and analysis. Vertical profiles of water temperature, salinity, and chlorophyll fluorescence were measured by AAQ-RINKO at 0.1 m intervals.

To visualize vertical distributions of *C. gigas* larvae, the weighted mean depth ($Depth_{mean}$) and weighted mean seawater density σ_t (σt_{mean}) were calculated at each sampling time as follows (Peteiro & Shanks 2015):

$$Depth_{mean} = \frac{\sum A_i z_i}{\sum A_i} \quad (1)$$

$$\sigma t_{mean} = \frac{\sum A_i \sigma t_i}{\sum A_i} \quad (2)$$

where A_i, z_i, and σt_i are the larval density, depth, and seawater density at the i^{th} sampling depth, respectively.

2.4. Monitoring of planktonic and settled larvae in Hiroshima Bay

To promote successful natural seedling collection in Hiroshima Bay, Hiroshima City Fisheries Promotion Center conducts frequent monitoring of planktonic and settled larvae in the morning (from 09:00 JST to 11:00 JST) mainly during July to August every year. In the present study, we used the data obtained in July 2020 to establish the initial condition of larval transport simulations as described in Section 2.7, and to validate the simulation results. At 10 monitoring stations in the northern area (Fig. 1), a plankton net (Kitahara's quantitative plankton net; mesh size 72 µm and 0.225 m diameter, Rigo) was towed vertically from a depth of 5 m to the surface; the obtained samples were immediately fixed with 37% (w/v) formaldehyde (the final formaldehyde concentration was 0.2%, w/v). To track abundance of each larval development stage, planktonic *C. gigas* larvae classified into 9 size classes, every 30 µm from ⩽90 to 300–330 µm, were directly counted under a microscope (BX43, Olympus). Information of larval abundance with each size class in each station has been provided to fishermen in quasi real-time to schedule seedling collection. As with Sections 2.2 and 2.3, the small size-class of larvae (⩽150 µm), estimated to be ⩽5 d post-fertilization, was used in this study. To monitor the abundance of settled larvae, spat collectors for seedling collection were placed at 0.3, 0.7, and 1.1 m depths at 10 stations in the northern area (northern Hiroshima Bay, Fig. 1) and at 5 others in the offshore area (near Ohkurokami Island; Fig. 1). The spat collectors were collected from the field the next day, transported to the laboratory, air dried, and the larvae that settled at the 3 depth layers were counted using a head loupe (Binocular magnifier, Vixen); then, we determined the average number of larvae that settled on spat collectors at the 3 depths.

2.5. Other environmental data and data analysis

Wind and solar radiation data recorded at the Hiroshima Meteorological Observatory (Fig. 1) were obtained from the Japan Meteorological Agency (www.jma.go.jp/jma/index.html). The sea level relative to Tokyo Peil (mean sea level at Tokyo Bay) at the Hiroshima port (Fig. 1) was provided by the Japan Ocean-

ographic Data Center (https://www.jodc.go.jp/jodcweb/index_j.html). The discharge from the Ohta River was obtained from the Ministry of Land, Infrastructure, Transport and Tourism, Japan (http://www1.river.go.jp/). These data were used to characterize the environmental conditions during cross-sectional and stationary observations. All statistical analyses, including Spearman's rank correlation, Welch's *t*-test, and regression (linear and quadratic functions), were performed using R version 4.0.4 (R Core Team 2021).

2.6. Hydrodynamic simulation

The hydrodynamic model is based on the Princeton Ocean Model; its configuration is described in detail by Abo & Onitsuka (2019). The model domain was 40 km east–west and 52 km north–south including Hiroshima Bay, with a horizontal resolution of 300 m and 21 sigma levels. Boundary conditions were provided by open boundaries with the water temperature, salinity, and sea level calculated by the Regional Ocean Modeling System around Japan (Kuroda et al. 2017). With respect to meteorological conditions, wind direction, wind speed, temperature, and relative humidity were given by the reanalysis data of GPV-MSM from the Japan Meteorological Agency. Precipitation data observed by the Japan Meteorological Agency were given at the surface layer as freshwater input to the hydrodynamic model. Major and minor rivers, including the Ohta River, were considered freshwater inflows into Hiroshima Bay. The model was integrated for 4 mo from 1 May to 31 August 2020. We evaluated the model performance that reproduced salinity and velocity fields (tidal and residual currents) during the rainy season when the heavy rainfall event occurred in July 2018 (Abo & Onitsuka 2019). The output every 0.5 h was used for particle-tracking experiments.

2.7. Lagrangian particle-tracking simulations

Lagrangian particle-tracking simulations were conducted using the velocity fields of the hydrodynamic model. The governing equations for the horizontal and vertical movements of particles simulating oyster larvae are as follows:

$$x_{t+\Delta t} = x_t + U\Delta t + R_x\sqrt{2K_h\Delta t} \quad (3)$$

$$y_{t+\Delta t} = y_t + V\Delta t + R_y\sqrt{2K_h\Delta t} \quad (4)$$

$$z_{t+\Delta t} = z_t + W\Delta t + K_v'\Delta t + R_z\sqrt{2K_v\Delta t} + \alpha W_{\mathrm{swim}}\Delta t - \left(1-\alpha\right)W_{\mathrm{sink}}\Delta t \quad (5)$$

where x, y, and z are the 3-dimensional positions of particles. U, V, and W denote the 3-dimensional velocities simulated by the hydrodynamic model, which were linearly interpolated in time and space to provide values at any particle location. Δt is the time interval (2 s). The advection of particles was calculated using the Euler-forward scheme. Random displacement was included in the particle-tracking model to simulate sub-grid scale turbulence (Visser 1997, North et al. 2006). R_x, R_y, and R_z are normal random numbers with standard deviation 1. K_h is the horizontal diffusivity coefficient at the particle location. K_v is the vertical diffusivity evaluated at (z_t + $0.5K_v'\Delta t$). K_v' equals $\partial K_v/\partial z$ evaluated at z_t. K_h and K_v were obtained from the hydrodynamic model. Based on the observations in the present study and previous studies on other oyster species (e.g. Dekshenieks et al. 1996, North et al. 2008), larval behavior in the vertical direction was considered (Eq. 5). W_{swim} and W_{sink} are the velocities of upward swimming and downward sinking, respectively. α is the fraction of time larvae swim, which is given as an input parameter for particle-tracking simulations. In the simulations, when the particles flowed out from the open boundary, such particles were removed. Landing of particles was avoided by moving the particles back to previous locations. Particles that moved outside the surface (or bottom) were put back the same distance vertically.

The swimming velocity of oyster larvae ranged from 0 mm s^{-1} to 2–6.5 mm s^{-1} as larvae develop from fertilized eggs to pediveligers (Hidu & Haskin 1978, Mann & Rainer 1990, Troost et al. 2008, Suquet et al. 2013, Gamain et al. 2020). According to the laboratory experiments in *C. gigas* larvae, swimming speeds were 0.146 mm s^{-1} for trochophores (Suquet et al. 2013) and 0.144–0.297 mm s^{-1} for D-larvae (Gamain et al. 2020). Troost et al. (2008) reported horizontal and vertical swimming speeds of 0.7–6.5 mm s^{-1} (size: 68–279 µm) and 0.9 mm s^{-1} (size: 173 µm), respectively. In the present study, we set the upward maximum swimming speed to increase linearly from 0.5 mm s^{-1} to 2.5 mm s^{-1} during the simulation period, based on the above laboratory studies and previous simulation studies with swimming speeds of 0–2.28 mm s^{-1} for *C. virginica* (Dekshenieks et al. 1996) and 0.5–3.0 mm s^{-1} for *C. virginica* and *C. ariakensis* (North et al. 2008). The maximum swimming speed was multiplied by a number drawn from a uniform random distribution between 0 and 1 to simulate random

variation in the movement of individual oyster larvae (North et al. 2008). The sinking velocity of oyster larvae increases approximately from 1 mm s^{-1} for small larvae up to 5 mm s^{-1} near settlement size (Hidu & Haskin 1978, Dekshenieks et al. 1996). Thus, we increased the downward sinking velocity from 1.0 mm s^{-1} to 5.0 mm s^{-1} during the simulation period. Previous studies adopted vertical larval behavior dependent on salinity (Dekshenieks et al. 1996, North et al. 2008). Dekshenieks et al. (1996) adopted an α of 0.64–0.83 (mean = 0.735) for *C. virginica* in response to salinity change. Based on field observations (Section 3.1), larval density peaked at approximately salinity 20 and decreased with decreasing salinity. We added vertical larval behavior that avoids low salinity. In the case of the control (Control), α was assigned a constant value of 0.81, except for salinity <20 at the position of the particle, resulting in a weak upward velocity of larvae on average. α linearly decreased from 0.81 to 0 at salinities ranging from 20 to 0; thus, all larvae sank at salinity of 0. The 3-dimensional salinity field from the hydrodynamic model was used to calculate vertical movements of particles simulating oyster larvae. The simulated salinity pattern reproduced 4 cross-sectional observations well, but the simulated salinity was higher than that observed as the salinity decreased. The bias between simulated and observed salinities was 3.7 at simulated salinity of 20. Therefore, the salinity field obtained from the hydrodynamic model was modified using the relationship between simulated and observed salinities ($n = 266$, $S_{obs} = 1.282\, S_{sim} - 9.38$, $R^2 = 0.773$, $p < 0.001$).

In addition to the abovementioned case of Control, 3 other case studies were conducted in particle-tracking simulations. Case 1 had no avoidance of low salinity (constant α value of 0.81). The other 2 cases considered diel swimming (Case 2) and tidal swimming (Case 3) following the results of 24 h stationary observation (see Section 3.2). In Case 2, vertical movement by a diel swimming speed of 0.05 mm s^{-1} (i.e. 2.16 m per 12 h) in a diurnal cycle (upward: 05:00–17:00 h JST, downward: 17:00–05:00 h JST) was added to Eq. (5). In Case 3, larvae swam upward during rising tides and downward during falling tides with a speed of 0.1 mm s^{-1}, which was added to Eq (5), corresponding with vertical migration (~2 m) in a semi-diurnal cycle. Considering avoidance from low salinity, upward swimming speeds were set to zero when salinity was below 20 in both Cases 2 & 3.

The initial particle positions were set in northern Hiroshima Bay (area NH, Fig. 1), which is the main spawning area in the bay. Ten particles were equally placed from 0 to 3 m depth at each horizontal grid cell (total number of particles: 17410). Particles simulating larvae had larval density information based on the monitoring data of small-sized larvae at 10 stations in northern Hiroshima Bay on 13 July 2020, as described in Section 2.4. The larval density in each horizontal grid cell was interpolated and extrapolated to area NH using a Gaussian filter with a radius of influence of 3 km. Thus, 10 particles vertically placed in each horizontal grid cell had the same larval density. The larval density of each particle did not change throughout simulations. The particle-tracking simulations were conducted for 9 d from 10:00 JST on 13 July when small-sized larvae rapidly increased in northern Hiroshima Bay to 10:00 JST on 22 July when settled larvae simultaneously increased in both northern Hiroshima Bay and the offshore area (the Ohkurokami Island area) (see Section 3.3). In the present simulations, we assumed that the larvae observed in the northern area on 13 July were transported and settled in both the northern and offshore areas on 22 July. The main larval size on 13 July was 90–120 µm (see Section 3.3), which was estimated at approximately 3–4 d post-fertilization (Arakawa 1990, Kusuki 2009). Thus, on 22 July, it took about 12–13 d post-fertilization, corresponding to a planktonic larval period of approximately 2 wk. The daily average distribution of particles simulating planktonic larvae was compared with the settled larval abundance obtained on 22 July (see Section 3.4).

3. RESULTS

3.1. Vertical distributions of *C. gigas* larvae and the relationship with environmental conditions

Although there were horizontal differences dependent on larval size, most larvae of all sizes were distributed in the surface layer throughout 4-time cross-sectional observations (Fig. 2). On 7 July 2020, the density of small and medium larval sizes was relatively high in the upper 3 m layer, except for the vertical profiles from Stns 1 to 3, where larvae were distributed throughout the water column, particularly for the small-sized larvae. The maximum densities were 4835 ind. 10 l^{-1} in small-sized larvae at Stn 2 on 21 July (Fig. 2C), 2414 ind. 10 l^{-1} in medium-sized larvae at Stn 2 on 16 July (Fig. 2F), and 691 ind. 10 l^{-1} in large-sized larvae at Stn 5 on 21 July (Fig. 2K). For small-sized larvae, the stations with maximum densities were distributed in northern Hiroshima Bay (Stns 1–4) in all sections (Fig. 2A–D). The abundance of medium and large-sized larvae was relatively high in the offshore area

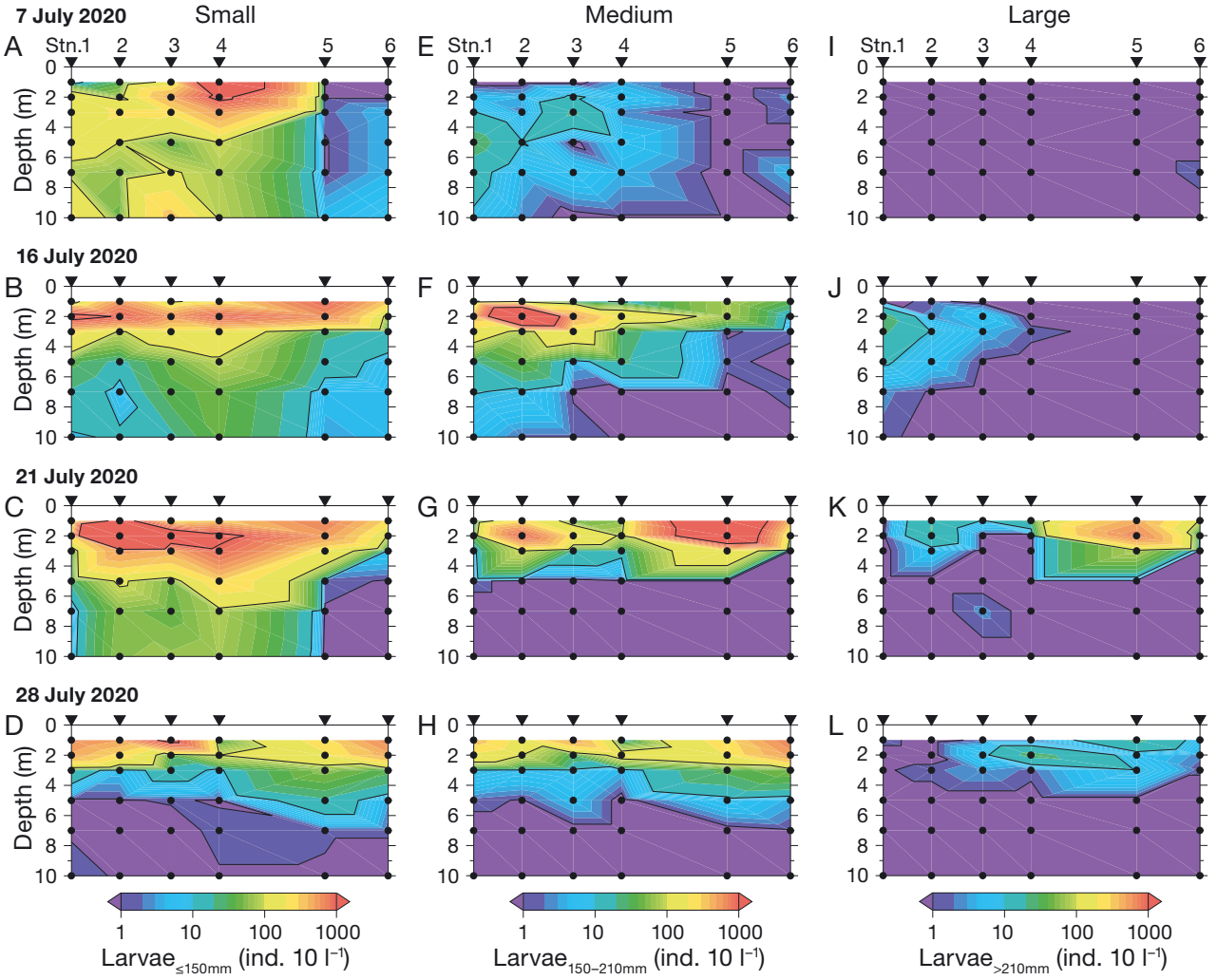

Fig. 2. Vertical sections of (A–D) small- (⩽150 µm), (E–H) medium- (150–210 µm), and (I–L) large-sized *C. gigas* larvae (>210 µm) along the line of Stns 1–6 on 7, 16, 21, and 28 July 2020. Closed circles indicate sampling depths; contour lines show base-10 exponential larval densities

(Stns 5 & 6) during the second half of the observation period on 21 and 28 July (Fig. 2G,H,K,L). The proportion of each size class of larvae found at each depth is shown in Fig. 3. More than 70% of the larvae for all size classes were distributed at 3 m or above. The maximum proportion of small-sized larvae was 0.36 at 2 m depth, and that of medium-sized larvae was 0.41 at 2 m depth and large-sized larvae was 0.32 at 1 m depth. Differences in proportions of larvae between salinities above and below 20 at 1 m depth were found at depths of 1 and 2 m for small and medium sizes and at depths of 1 and 3 m for large size. Differences were not significant at 1 m depth because of the large standard deviations (Welch's *t*-test, small size: $t = 1.955$, df = 17.62, $p = 0.067$, medium size: $t = 1.435$, df = 17.06, $p = 0.169$, large size: $t = 1.017$, df = 13.33, $p = 0.327$), but significant at 2 m depth for small and medium sizes (Welch's *t*-test, small size: $t = 2.483$, df = 21.72, $p = 0.021$, medium size: $t = 2.283$, df = 21.34, $p = 0.033$). The proportions of larvae with salinity >20 at 1 m depth increased monotonically as it became shallower.

During the observation period in July 2020, water temperature, salinity, and chl *a* concentration changed, especially in the upper 4 m layer (Fig. 4). The lowest and highest water temperature, salinity and chl *a* concentration across all cruises varied in the range of 19.9–28.3°C, 2.5–31.7, and 0.8–30.5 µg l^{-1}, respectively. Thermoclines and/or haloclines were distributed around 2–3 m depth. Additionally, the distribution patterns of water temperature and salinity barely changed deeper than 4 m depth among cross-sections. After the high river discharge on 14 July (Fig. S1 in the Supplement at www.int-res.com/articles/suppl/m740p043_supp.pdf), low salinity ⩽20 expanded to the offshore area on 16 July. Afterward, the water temperature increased in the surface low-salinity

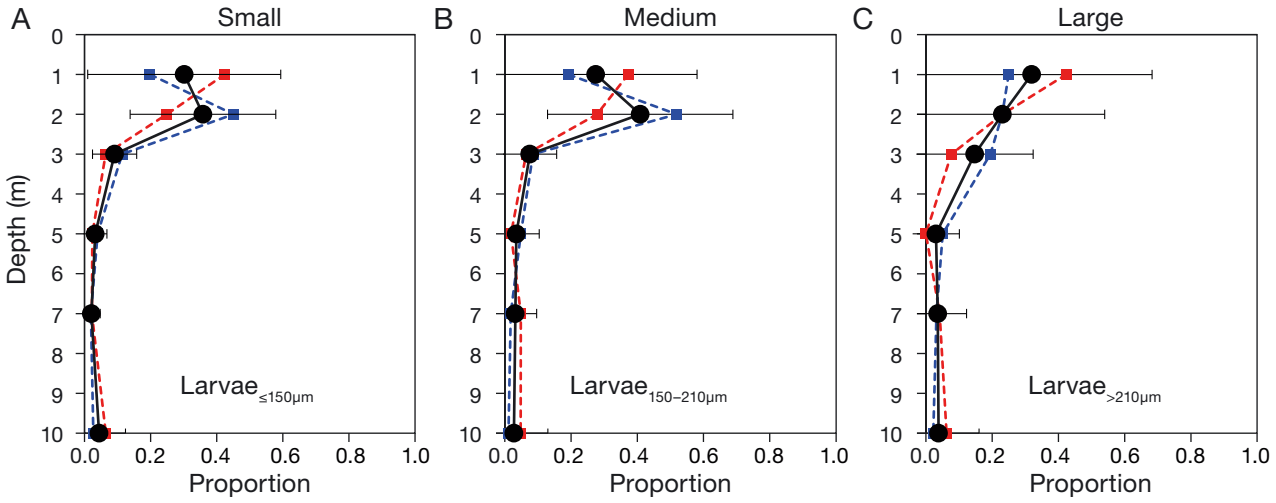

Fig. 3. Normalized vertical profiles of (A) small- (⩽150 µm), (B) medium- (150–210 µm), and (C) large-sized *C. gigas* larvae (>210 µm) during cross-sectional observations. Black circles and bars indicate mean ± SD at the respective depths. Red and blue squares indicate the mean proportions of larvae at each depth when salinity at 1 m depth is above or below 20, respectively

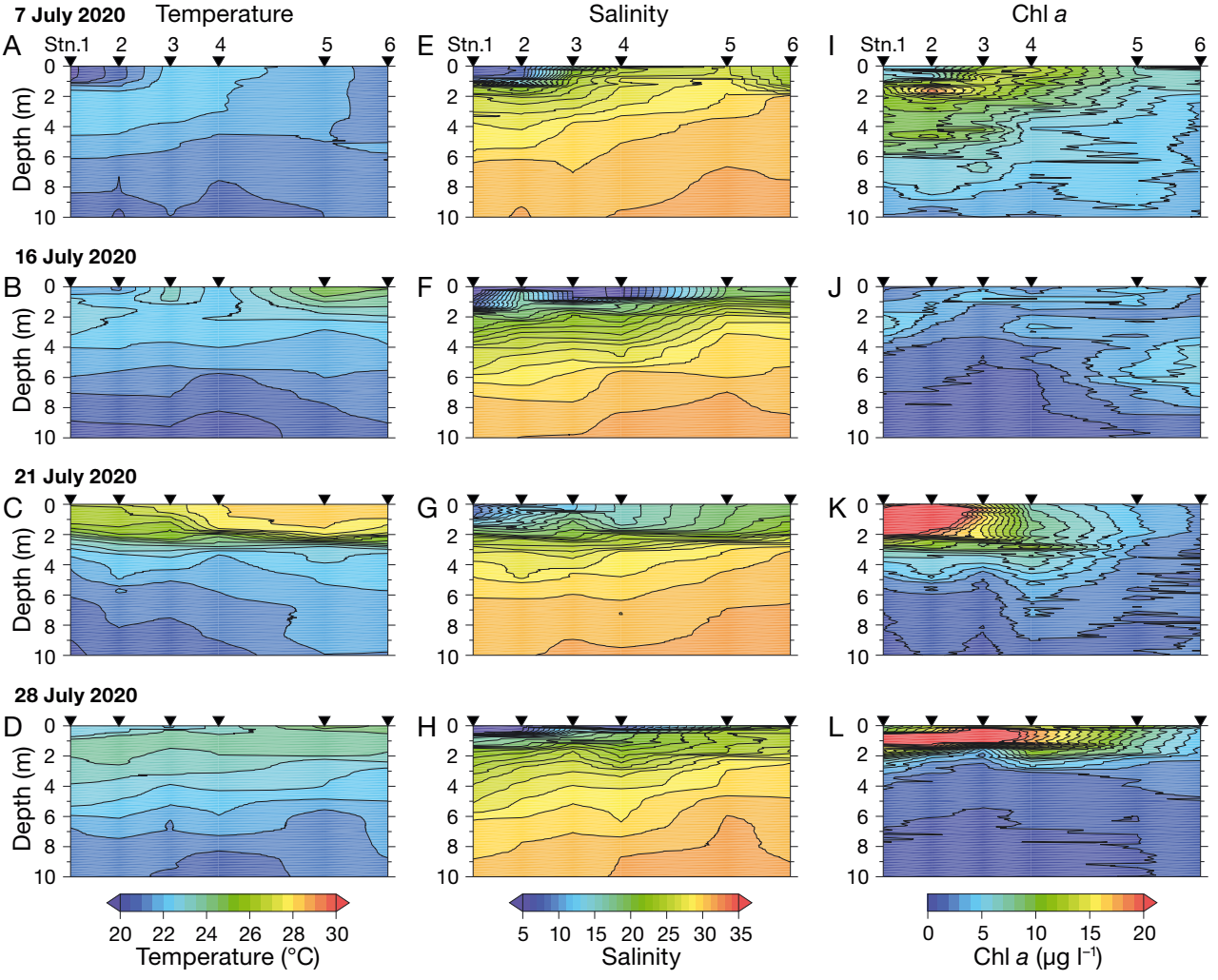

Fig. 4. Vertical sections of (A–D) water temperature, (E–H) salinity, and (I–L) chlorophyll *a* concentration along the line of Stns 1–6 on 7, 16, 21, and 28 July 2020. Contour intervals for temperature, salinity and chl *a* are 0.5°C, 1, and 1 µg l^{-1}, respectively

water due to surface heating caused by air temperature and solar radiation. In addition, high chl *a* concentration >20 µg l^{-1} was observed in the surface layer at Stns 1 and 2 near the river mouth on 21 and 28 July.

The relationship between logarithmic larval density and environmental conditions observed in the cross-sectional observations is shown in Fig. 5. Larval density increased with increasing temperature. There were significantly positive correlations between temperature and all size classes (Spearman's rank correlation, small size: n = 144, ρ = 0.522, p < 0.001, medium size: n =144, ρ = 0.699, p < 0.001, large size: n = 144, ρ = 0.465, p < 0.001). Significantly positive correlations were found between logarithmic larval density and chl *a* concentration, except for large-sized larvae (Spearman's rank correlation, small size: n = 144, ρ = 0.533, p < 0.001, medium size: n =144, ρ = 0.410, p < 0.001, large size: n = 144, ρ = 0.119, p = 0.156). On the other hand, despite the significantly negative correlations between logarithmic larval density and salinity (Spearman's rank correlation, small size: n = 144, ρ = −0.584, p < 0.001, medium size: n =144, ρ = −0.653, p < 0.001, large size: n = 144, ρ = −0.451, p < 0.001), larval densities drastically decreased at salinity <15 in all size classes. The relationship between logarithmic larval density and salinity was approximated by a quadratic function (Fig. 5D–F). Based on the quadratic function in each size class, larval densities in small, medium, and large sizes peaked at salinities of 20.0, 19.8, and 19.4, respectively.

3.2. Diurnal/semi-diurnal changes in vertical distribution

Although larval density varied at an hourly time scale, most larvae were distributed in the surface layer as observed during the cross-sectional observations (Fig. 6A,B). The maximum density was 3240 ind. 10 l^{-1} for small size and 10.2 ind. 10 l^{-1} for medium–

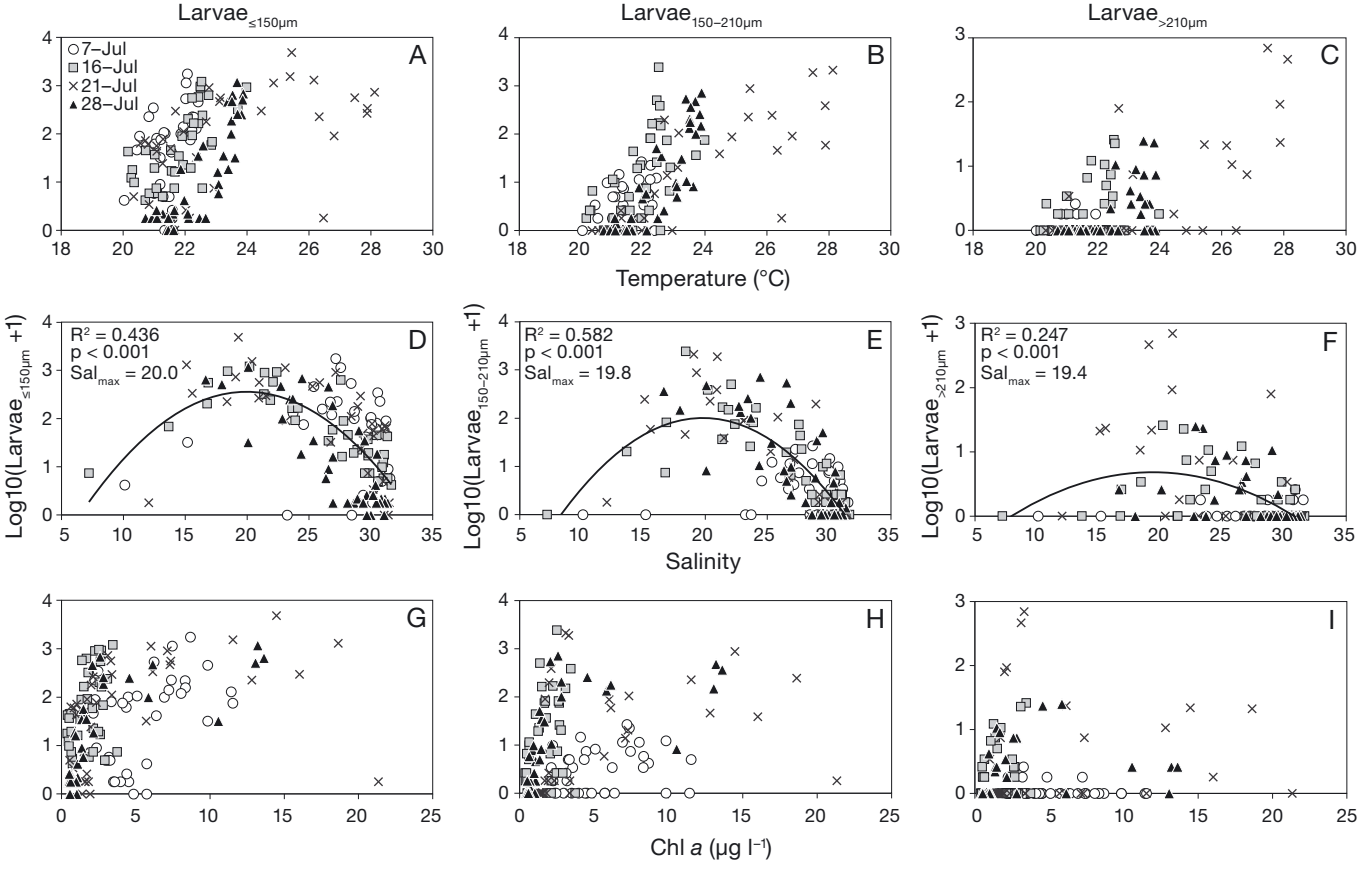

Fig. 5. Relationships between *C. gigas* larval density in 3 size classes and (A–C) water temperature, (D–F) salinity, and (G–I) chlorophyll *a* concentration during cross-section observations. Open circles, grey squares, crosses, and closed triangles indicate values on 7, 16, 21, and 28 July 2020, respectively. The regression curves of quadratic functions for salinity are drawn in scatter plots

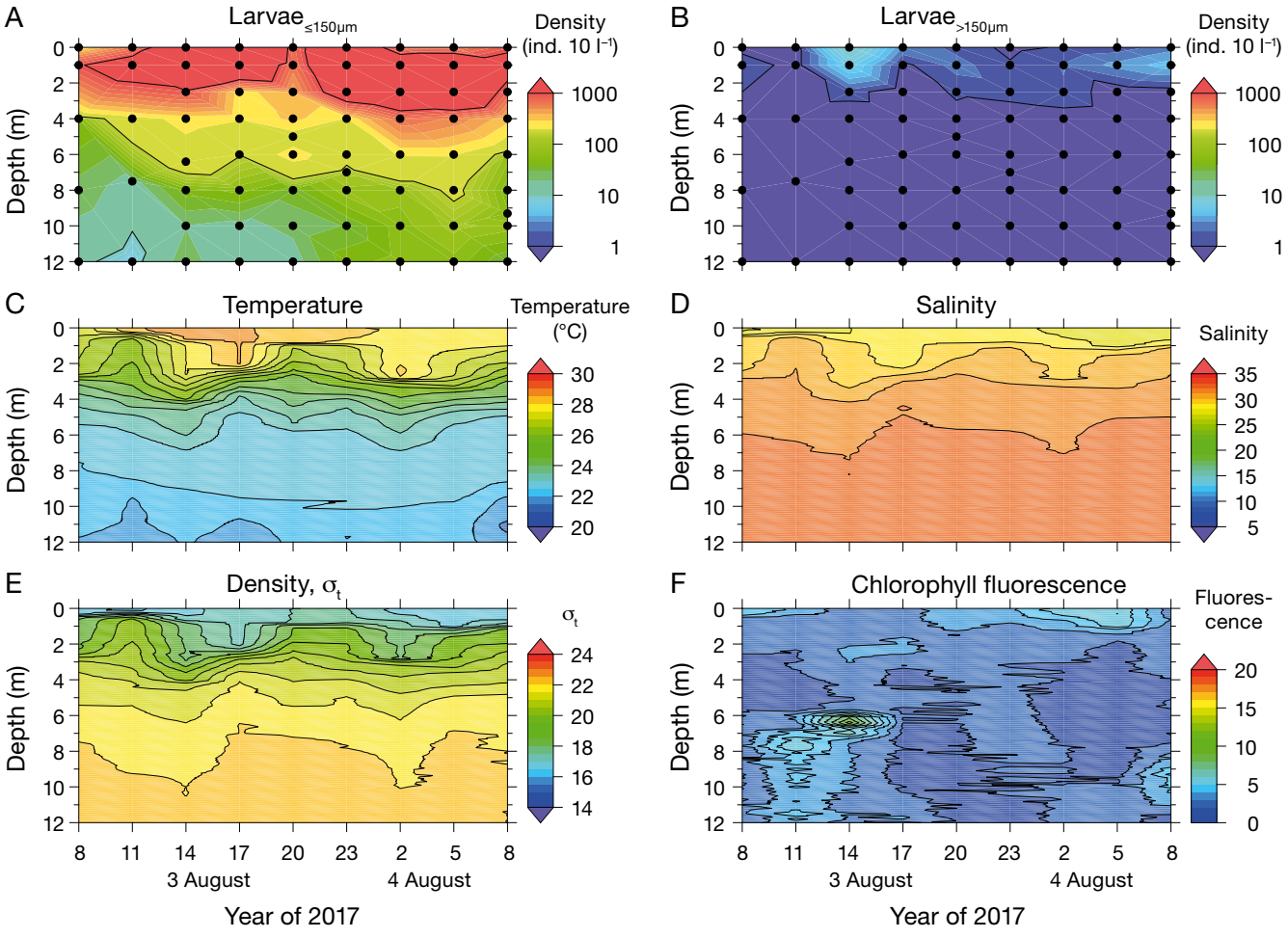

Fig. 6. Vertical distribution of (A, B) *C. gigas* larvae (small: ⩽150 µm, medium–large: >150 µm), (C) water temperature, (D) salinity, (E) seawater density σ_t, and (F) chlorophyll fluorescence at Stn 3 over 24 h on 3–4 August 2017. Contour lines of larvae show exponential densities. Closed circles in (A,B): sampling depths. Contour intervals for water temperature, salinity, σ_t, and chlorophyll fluorescence increment by 0.5°C, 1, 1, and 1, respectively

large size larvae over 24 h. Water temperature and salinity in the upper 5 m depth showed cyclic changes corresponding with semi-diurnal tides, resulting in semi-diurnal vertical pycnocline displacement (Fig. 6C–E; Fig. S2 in the Supplement). Chlorophyll fluorescence remained low at <10.5 throughout the observation (Fig. 6F).

The depths of the maximum and mean larval distributions were ⩽3 m for both small and medium–large sizes, with diurnal changes (Fig. 7A,B). The depths were shallower in the afternoon and deeper from midnight to the early hours in the morning. On the other hand, the seawater density σ_t with maximum and mean larval densities showed a semi-diurnal cycle, particularly for medium–large sized larvae (Fig. 7C,D). Low σ_t roughly corresponded with the flood tide (Fig. 6E; Fig. S2).

3.3. Temporal dynamics of planktonic and settled larvae in July 2020

In northern Hiroshima Bay (Fig. 1), small-sized planktonic larvae remained at low densities, <10 ind. 10 l^{-1} in early July 2020, but rapidly increased from 38 ind. 10 l^{-1} on 9 July to 413 ind. 10 l^{-1} on 13 July (Fig. 8). According to the Hiroshima City Fisheries Promotion Center, the main larval size was 90–120 µm on 13 July. Settled larval abundances in the northern area and the offshore area (the Ohkurokami Island area; Fig. 1) continued to be low, <5 ind. $plate^{-1}$ d^{-1} until 20 July, but rapidly increased at the same time from July 21. The settled larvae averaged over both areas were 91 ind. $plate^{-1}$ d^{-1} in the northern area and 113 ind. $plate^{-1}$ d^{-1} in the offshore area on 22 July. The settled larval abundances at the stations in the

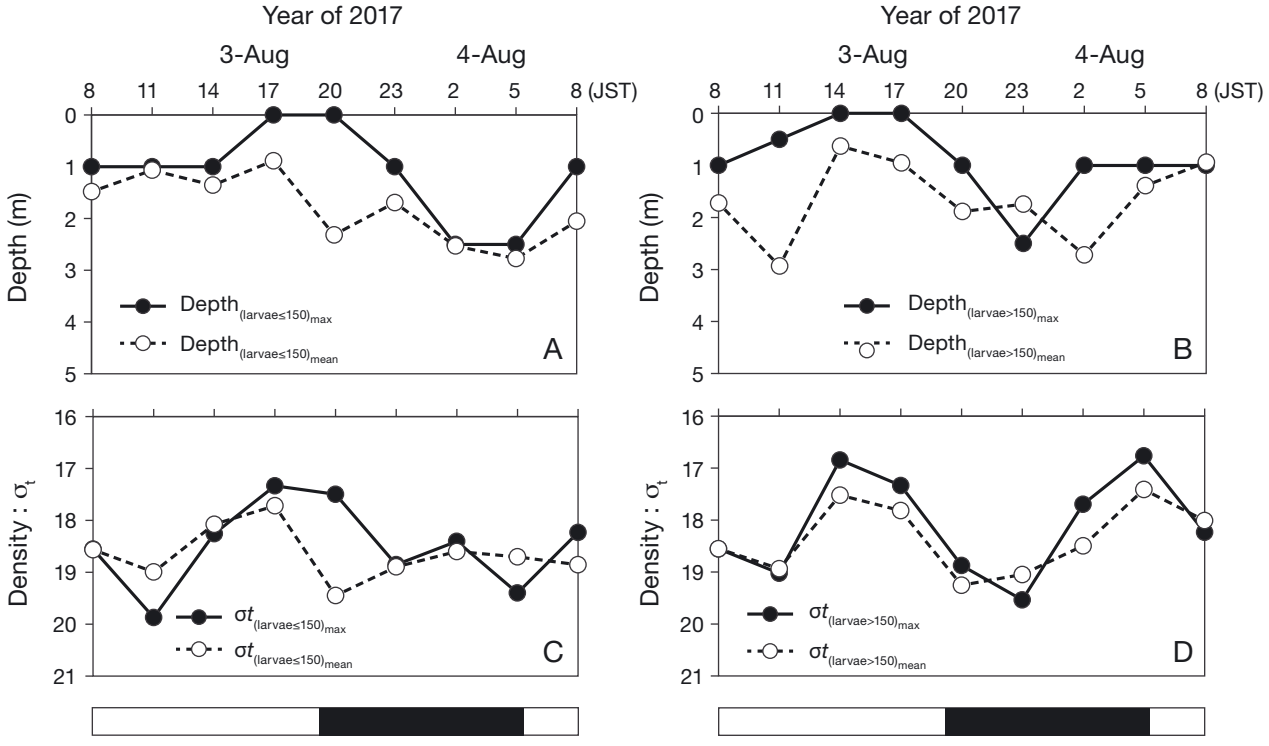

Fig. 7. Upper panels show temporal changes in depth of the maximum larval density (solid line and closed circles) and weighted mean depth (broken line and open circles) with (A) small (⩽150 µm) and (B) medium–large sized *C. gigas* larvae (>150 µm) for 24 h on 3–4 August 2017. Lower panels show temporal changes in seawater density σ_t of the maximum larval density (solid line and closed circles) and weighted mean σ_t (broken line and open circles) with (C) small (⩽150 µm) and (D) medium–large sized *C. gigas* larvae (>150 µm). Open and solid bars below the horizontal axes represent daytime and nighttime, respectively

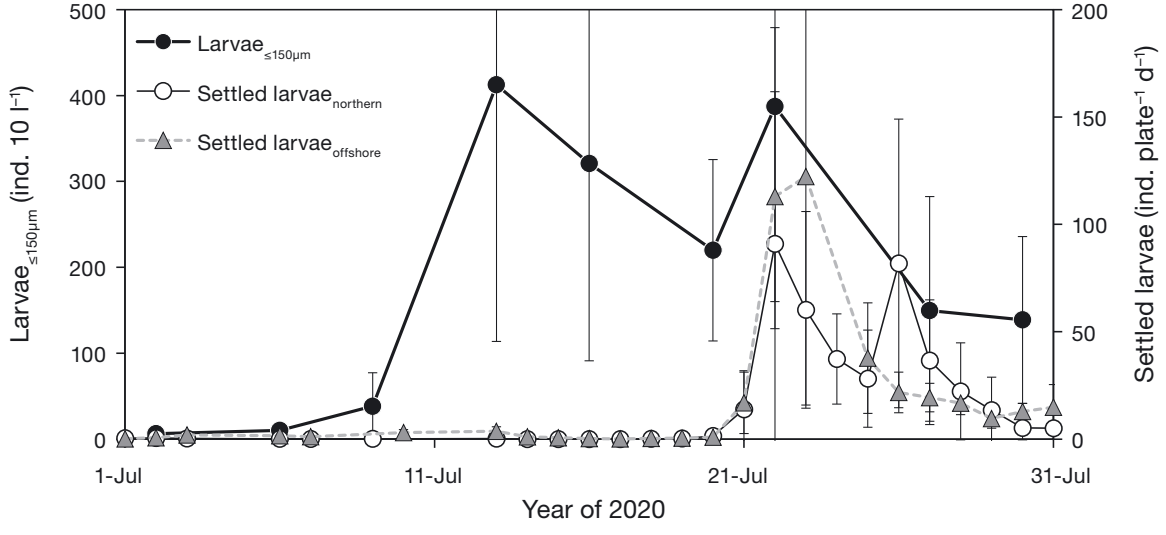

Fig. 8. Temporal changes in small-sized larval density in the northern area (thick solid line and closed circles), and in settled larvae in the northern area (thin solid line and open circles) and offshore area (grey broken line and grey triangles) in July 2020. Plus and cross symbols presented in Fig. 1 indicate the monitoring stations in the northern area and offshore area, respectively. Symbols and bars indicate mean ± SD among stations in each area

northern area had a positive correlation with pediveliger larvae (>270 µm) observed by the Hiroshima City Fisheries Promotion Center at the same stations on 22 July (Spearman's rank correlation, n = 10, ρ = 0.636, p = 0.054).

3.4. Numerical simulations of hydrodynamic conditions and larvae-simulating particles

Low-salinity water extended to a broad area in the surface layer of northern Hiroshima Bay on 16 July 2020 (Fig. 9B), when simulation elapsed 3 d after the start on 13 July due to high discharge of the Ohta River on 14 July (Fig. S1). Low-salinity water moved southward along the coastal area in Hiroshima Bay. Then, southward currents appeared in the surface layer throughout the simulation (Fig. 9A–D). In particular, high velocity occurred from the river mouth of the Ohta River to the southern coast of the Miyajima Island. Despite discrepancies between the simulated and observed values, the simulated vertical distributions of water temperature and salinity captured the distribution patterns observed in 4-time cross-sectional observations (Figs. 4A–H; Fig. S3 in the Supplement).

Most particles simulating planktonic larvae outflowed from the northern area through the Ohno, Nasabi, and Kure Straits during the simulation period (Fig. 9E–H). About 60% of particles in area NH were lost on 16 July, 3 d after the start of particle-tracking simulation. The horizontal distribution of particles outside the straits corresponded with the extent of low salinity on 16 July. Some particles through the straits had large dispersion of >10 km d^{-1}. On 19 July, >80% of particles outflowed from area NH. However, such particles reached the area around Ohkurokami Island, which was consistent with the extent of low salinity. At the end of the simulation on 22 July, 4.3% of particles remained in area NH. The proportion of simulated particles in each depth layer is shown in Fig. 10. The maximum number of particles was observed in the subsurface layer (1–3 m depth) on 16 July when the surface salinity <20 extended to a broad area of northern Hiroshima Bay (Fig. 9B). The vertical profile was qualitatively consistent with that observed for small- and medium-sized larvae (Fig. 3A,B). In contrast, there was a surface maximum of particles simulating larvae on 22 July when salinity became saltier in the surface layer, corresponding to the profile for large-sized larvae in Fig. 3C.

The daily average distribution of particles simulating planktonic larvae and the settled larval abundance obtained on 22 July are shown in Fig. 11. Except for the semi-enclosed inlets in the northwestern NH, high densities of simulated larvae were distributed in the southern part of NH and in offshore areas, especially around Ohkurokami Island, where oyster farmers traditionally conduct seedling collection. The spatial pattern of settled larvae on 22 July was consistent with the simulated larval density. There was a significant correlation between settled larvae and simulated larval density (Spearman's rank correlation: n = 15, ρ = 0.538, p = 0.041). According to independent monitoring of oyster farmers, there was a high density of larval settlement (100 ind. $plate^{-1}$ d^{-1}) in the southwestern area of Miyajima Island (Hiroshima Fishery Cooperative unpubl.), corresponding to the high density of simulated planktonic larvae.

We also evaluated the differences in the cases with different swimming behaviors (Fig. 12). In the case without avoidance from low salinity ⩽20 (Case 1), the proportion of particles remaining in area NH decreased faster than that with low-salinity avoidance (Control) just after the high river discharge on 14 July. The particles remaining in area NH in Case 1 were about half of the Control case on 17 July. The proportion in cases with diurnal or semi-diurnal changes (Cases 2 & 3) over time was higher than the case of Control. At the end of the simulations at 10:00 h JST on 22 July, the proportions were 3.1% for Case 1, 5.4% for Case 2, and 4.9% for Case 3. The daily average distributions of particles with larval density in Cases 1–3 on 22 July showed similar patterns to the Control case shown in Fig. 11. Spearman's rank correlations between the cases of Control and Case 1, Control and Case 2, and Control and Case 3 were 0.925 (n = 15, p < 0.001), 0.954 (n = 15, p < 0.001), and 0.904 (n = 15, p < 0.001), respectively.

4. DISCUSSION

4.1. Vertical distribution characteristics of *C. gigas* larvae

Field observations in July 2020 showed the vertical distributions of *C. gigas* larvae and the relationship with environmental conditions. This period was suitable for the observation of various larval sizes due to the presence of early-stage and settled larvae. Despite horizontal differences depending on larval size, most larvae were distributed in the upper 3 m layer. Surface distribution through a planktonic stage seems to be a fundamental trait of *C. gigas* larvae, as the mean depth was distinctively shallow compared with other oyster species (Kennedy 1996, Peteiro & Shanks 2015). In northern Hiroshima Bay, nutrients from the Ohta River

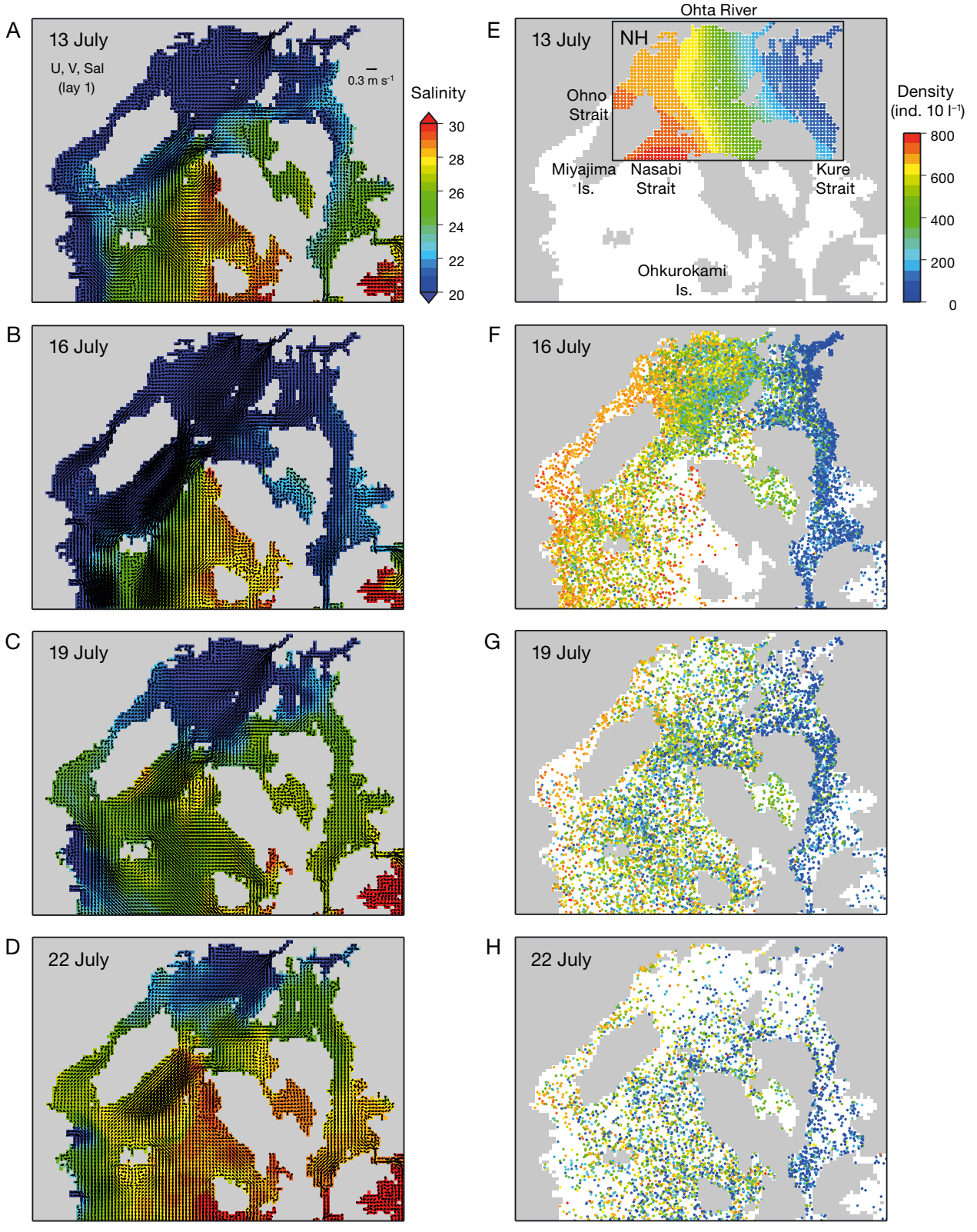

Fig. 9. Simulated distributions of (A–D) velocity and salinity fields in the 1st sigma layer (i.e. surface layer) and (E–H) particles simulating larvae at 10:00 JST on 13, 16, 19, and 22 July 2020. Velocity fields are averaged over 25 h from 21:30 JST to 22:30 JST each day. NH (rectangular area) indicates the initial particle position in northern Hiroshima Bay. Particle color represents small-sized (⩽150 µm) larval density calculated from monitoring data on 13 July 2020

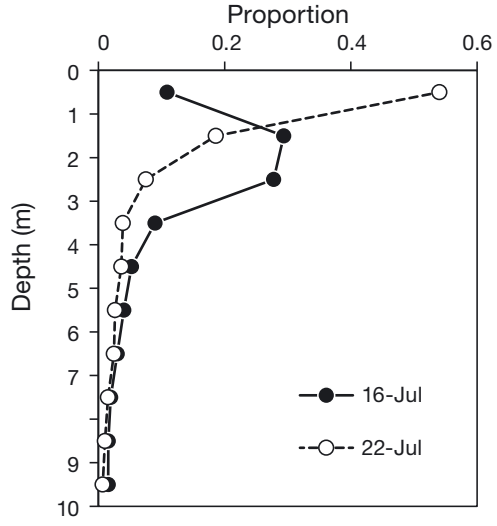

Fig. 10. Normalized vertical profiles of simulated particles in area NH (area with depth >10 m) at 10:00 JST on 16 and 22 July 2020

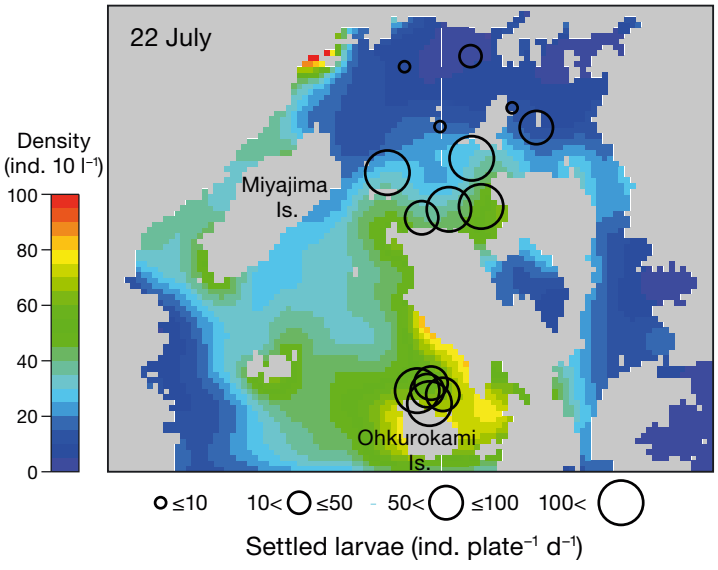

Fig. 11. Daily averaged distribution of particles simulating larvae from 10:00 JST on 21 July to 10:00 JST on 22 July 2020, and distribution of settled larvae on 22 July 2020 (open circles). Horizontal distribution of particles simulating larvae in the water column was smoothed using a Gaussian filter with a radius of influence of 1 km. Larval density was multiplied by 0.1 because the initial number of particles per grid cell was 10

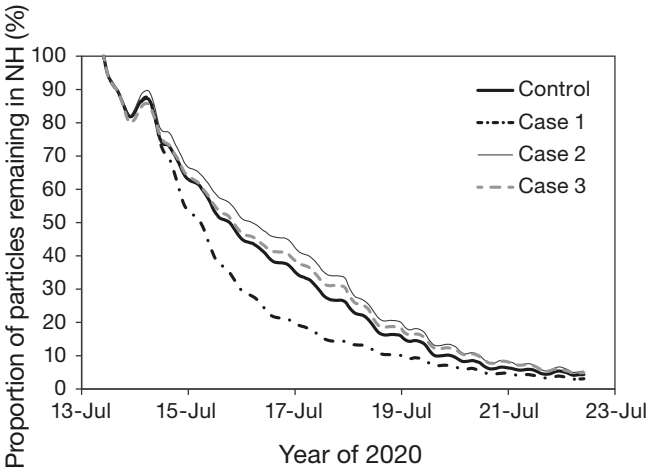

Fig. 12. Temporal changes in the proportions of particles simulating larvae remaining in area NH in 4 cases from 10:00 JST on 13 July to 10:00 JST on 22 July 2020

provide good feeding conditions for larvae (Wahyudin & Yamamoto 2020, Matsubara et al. 2023). Chl *a* concentration increased to >20 µg l^{-1} in the latter half of July, which significantly correlated with the larval density of small and medium sizes. Matsubara et al. (2023) identified high water temperature (>26.9°C) and high density of <10 µm size phytoplankton (chl *a* concentration >5 µg l^{-1}) as factors for successful larval settlement. Our results suggest that the vertical distribution characteristics of *C. gigas* larvae are suitable for survival in an estuarine area, where environmental conditions are potentially favorable.

However, larval distribution in the surface layer has a disadvantage that larvae cannot sufficiently remain in favorable environmental conditions due to outflow from the northern area in the rainy season. In Matsushima Bay, one of the major oyster farming areas in Japan along with Hiroshima Bay, freshwater input accelerated the outflow of oyster larvae in 2013, resulting in significant decline of seedling collection (Kakehi et al. 2016). In our simulations, many particles were transported from northern Hiroshima Bay by southward density-driven currents after high river discharge. However, the relationship between larval density and salinity suggest that this might reduce larval outflow. The density peaked at a salinity of approximately 20 for all larval sizes, with fewer larvae being found at low salinity (<15). The peak salinity found here was somewhat lower than the optimum salinity range (23–28) described in a previous study (Fujiya 1970). Small- and medium-sized larvae, which were abundant in the northern area, occupied a relatively small proportion at 1 m depth compared with the maximum proportion at 2 m. Differences in the proportion of larvae between salinities above and below 20 in the upper 2 m layer suggest consequential low-salinity avoidance of *C. gigas* larvae. Although the surface decrease in large-sized larvae was not distinct, which is possibly because the horizontal distribution shifted to offshore, the proportion with salinity below 20 was lower than that with salinity above 20 at 1 m depth. In fact, the larval abundance proportion at 1 m depth in the normalized vertical profile had a positive correlation with salinity observed at 1 m depth for all larval sizes collected by the cross-sectional

observations after the high river discharge on 14 July 2020 (Spearman's rank correlations, small size: $n = 18$, $\rho = 0.748$, $p < 0.001$, medium size: $n = 18$, $\rho = 0.653$, $p = 0.004$, large size: $n = 18$, $\rho = 0.529$, $p = 0.029$). Consequently, avoidance of low salinity is likely to have reduced the larval outflow induced by the high velocity of density-driven currents in the surface layer.

Avoiding low salinity below 20 seems to be one of the important survival strategies of *C. gigas* larvae to remain in the area where feeding condition is potentially favorable as previously described. We evaluated this process through simulations with and without avoidance from low salinity. In the case without avoidance from low salinity (Case 1), the proportion of particles remaining in area NH decreased faster than in that with low-salinity avoidance (Control), indicating the retention of *C. gigas* larvae in the northern area due to avoidance of low salinity. The proportion of retention in the northern area is likely dependent on the magnitude of river discharge. In July 2018, when heavy rainfall occurred and then low salinity <20 continued for >2 wk in the northern area, larval settlements remained at a high level after late July (Abo & Onitsuka 2019, Matsubara et al. 2023). In addition, considering the relatively large impact of feeding conditions on small-sized larvae such as D-shaped larvae (His & Seaman 1992, Matsubara et al. 2023), the effect of low-salinity avoidance may depend on the timing between salinity decrease and fertilization. Further, Kimura et al. (1975) suggested that southward wind can accelerate larval outflow. In the present study, the simulation period was fixed, 13–22 July 2020, when northward wind dominated. Additional simulation studies with sensitivities of hydrodynamic conditions during other periods are necessary to evaluate the impact of retention. Nevertheless, the present study implies that the vertical distribution characteristics of *C. gigas* larvae enables a large dispersion of >10 km day^{-1}, but larvae occasionally have the ability to remain in a particular area.

Although it should be noted that 24 h sampling was not replicated, diurnal changes in vertical larvae distribution were detected over the 24 h observation period. The maximum and mean depths were shallow in the afternoon and deep from midnight to the early hours in the morning in both small and medium–large sizes, indicating diel vertical migration, but a different vertical rhythm compared with the normal nocturnal ascent and daytime descent (Garland et al. 2002, Kunze et al. 2013). The pattern observed in the present study may be reverse diel vertical migration (Poulin et al. 2002). Medium–large sized larvae also showed a semi-diurnal cycle with respect to seawater density, with a rhythm synchronized to the semi-diurnal tide. Previous studies suggested the relationship with rising and falling tides (Kennedy 1996, Peteiro & Shanks 2015). Another possible cause for diurnal/semi-diurnal changes is the advection of water masses reflecting the different larval profiles. Considering the horizontal difference in larval distribution, apparent temporal change may be due to the advection at the fixed point. As mentioned above, as the 24 h sampling was not replicated in the present study, additional research is needed to elucidate diurnal/semi-diurnal variation. As for particle-tracking simulations, diurnal/semi-diurnal changes did not markedly affect the results, probably due to the small vertical movement.

4.2. Spatio-temporal dynamics of *C. gigas* larvae in Hiroshima Bay

The vertical distribution characteristics of *C. gigas* larvae observed in the present study were used for numerical modeling of this species. The high density of particles from northern Hiroshima Bay to the southern area of the Miyajima Island on 16 July 2020 were consistent with larval density observed after high river discharge (Kusuki et al. 1992). The larval profiles on 16 and 22 July roughly corresponded to those obtained in the cross-sectional observations and the spatial pattern of daily averaged particles reproduced the horizontal pattern of larval settlements. These results suggest the diagnostic validity with regards to setting of model parameters for larval vertical motions and the simulation period. Modeling for other oyster species such as *C. virginica* adopted a larval behavior which includes movement to deep layers in the latter half of their planktonic larval stage (Dekshenieks et al. 1996, North et al. 2008), implying that the behavior is species-specific and the behavior of other species cannot reproduce the spatio-temporal dynamics of *C. gigas* larvae, especially in offshore areas of Hiroshima Bay.

The correspondence between larvae-simulating particles and settled larval abundance indicates that larval population spawning in oyster farms discretely located in the northern area contribute to seedling collection in the offshore area around Ohkurokami Island set up by oyster farmers. The areas for seedling collection have empirically added the Ohkurokami Island area since the 1990s (Hirata et al. 2006). The present simulation indicates that this empirical countermeasure for failure of seedling collection is efficient, based on the dispersion strategy of *C. gigas* larvae.

In northern Hiroshima Bay, Matsubara et al. (2023) evaluated the ratio of settled larvae after 8–12 d to D-shaped larvae (<4 d old) as a settlement index. They identified a positive correlation with water temperature and chl *a* concentration for <10 µm size phytoplankton, suggesting that these factors are necessary for larval survival. As the index includes not only biological loss but also larval dispersion, quantification of larval dispersion enables a more accurate estimation of biological loss (i.e. mortality rate) of larvae. From field monitoring data, the ratio of pre-attached larvae (>270 µm) on 22 July to small-sized larvae (≤150 µm) on 13 July was 0.3% in the northern area (mean of 10 stations), which was within the range of the recent seasonal average ratio of 0.1–1.0% (Kusuki 2009). The rate of larval decrease over 9 d was 0.65 d^{-1}. On the other hand, the rate of decrease by dispersion was 0.35 d^{-1} based on the simulation results (Control case) in the northern area on 13 and 22 July. Consequently, the mortality rate of larvae was estimated as 0.30 d^{-1}, lower than 0.43 d^{-1} obtained by Kakehi (2022) but higher than 0.1–0.172 d^{-1} in most simulation studies (Dekshenieks et al. 1997, Hofmann et al. 2004, Kakehi et al. 2020, Wahyudin & Yamamoto 2020). According to Matsubara et al. (2023), the settlement index was low in the middle of July 2020, possibly due to the bloom of the harmful raphidophyte *Heterosigma akashiwo*. Our simulation results suggest that larval dispersion was comparable to the biological loss in this period. A combination of field monitoring and numerical simulations could serve to reveal the main causes for failure of seedling collection from biological and physical aspects.

As mentioned in Section 1, the application of numerical models to *C. gigas* is limited to either experiments with various assumptions of vertical behavior (Robins et al. 2017) or calculations that incorporate the biological characteristics of other oyster species (Kakehi et al. 2020). The biological characteristics of *C. gigas* larvae obtained in the present study can be utilized to evaluate larval recruitment of this species worldwide. The present simulation is a first attempt to incorporate the vertical distribution characteristics of *C. gigas* larvae; therefore, the attempt provides broader implications for our findings beyond Hiroshima Bay.

4.3. Prospects for sustainability in oyster aquaculture with respect to seedling collection

According to the Sixth Assessment Report (AR6) of the Intergovernmental Panel on Climate Change (IPCC), heavy rainfall has become more frequent and intense across parts of the world including East Asia; an event which will tend to increase with global warming (Clarke et al. 2022). As mentioned above, *C. gigas* larvae avoid low salinity, but there is a concern about negative impact of heavy rainfall on seedling collection. Fig. 13 illustrates the relationship between precipitation in July and the proportion of seedling collection in Hiroshima Bay. Failure of seedling collection, i.e. proportion of seedling collection <80%, did not occur in years of high precipitation >300 mm in July, indicating that outflow caused by high river discharge is not a likely threat for seedling collection in Hiroshima Bay. In the case of high river discharge, although most larvae quickly outflow from the northern area, countermeasures by oyster farmers and local governments, such as setting offshore seedling collection areas and the northward movement of rafts for adult oysters, contribute to sustainability in oyster aquaculture in Hiroshima Bay. In fact, seedling collection was successful in July 2018, when heavy rainfall occurred around the area (Abo & Onitsuka 2019). Nevertheless, attention is required to the indirect impact of heavy rainfall on seedling collection. The increase in heavy rainfall may enhance stratification and result in oxygen deficiency in summer (T. Yamamoto et al. 2011, H. Yamamoto et al. 2021). High precipitation decreases not only salinity but also pH and aragonite saturation state in the coastal area of the Seto Inland Sea (Fujii et al. 2023, Ono et al. 2024).

As Sustainable Development Goal 14 (SDG14) calls for sustainable management of marine and coastal ecosystems, oyster farming with no feed inputs has also been reported to contribute to the maintenance

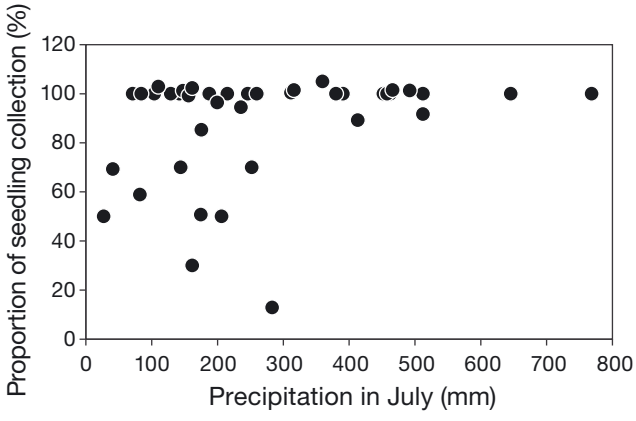

Fig. 13. Relationship between monthly precipitation in July and the proportions of seedling collection in Hiroshima Bay from 1980 to 2021. Proportions of seedling collection were recorded by the Hiroshima Prefecture, and are calculated by comparing the spat collections obtained each year against the predicted needs of fishermen. Collections occasionally exceed the predicted needs; thus, the proportion could be >100%

and improvement of coastal environments (Ray & Fulweiler 2021). The aquaculture of Pacific oyster is expected to become an important source of food security, because the species is farmed in many coastal areas around the world. The larval ecology, simulation results and methodologies described in the present study provide important insights that contribute to sustainable aquaculture. In the Seto Inland Sea, including Hiroshima Bay, the most intensive oyster farming area in Japan, cultural oligotrophication due to nutrient reduction has recently become problematic (Yamamoto 2003, Abo & Yamamoto 2019). The relationship between decreasing nutrients and decreased fisheries production has been highlighted by Abo & Yamamoto (2019). In Hiroshima Bay, the relationship among nutrients, phytoplankton as larval food, and *C. gigas* larvae was analyzed using field data (Matsubara et al. 2023) and a prey–predator model (Wahyudin & Yamamoto 2020, Yamamoto et al. 2023). These studies commonly emphasized the importance of larval food conditions. In a Mediterranean lagoon where oligotrophication has also occurred, Lagarde et al. (2017) also identified high abundances of nanophytoplankton and the diatom *Chaetoceros* spp. as favorable conditions for recruitment. Lagarde et al. (2019) evaluated the processes that drive spatial patterns in oyster recruitment by comparing spat collection data, simulated hydrodynamic connectivity, and ecological variables. Comparisons of hydrodynamic connectivity and feeding conditions among oyster farms using numerical models will aid in the efficient collection of seedlings, such as through the careful location of oyster rafts.

Acknowledgements. The authors thank the captains and crews of RV Shirafuji-maru of Japan Fisheries Research and Education Agency and RV Dai-kyu Shisui-maru of Hiroshima City. We are grateful to Dr. Yoichi Miyake for useful discussions. This study was funded in part by grants from Japan Fisheries Research and Education Agency, Hiroshima Prefecture and Hiroshima City.

LITERATURE CITED

Abo K, Onitsuka G (2019) Characteristic of currents induced by heavy rainfall in Hiroshima Bay in July 2018. J Jpn Soc Civ Eng B2 75:I_1051–I_1056 (in Japanese with English abstract)

Abo K, Yamamoto T (2019) Oligotrophication and its measures in the Seto Inland Sea, Japan. Bull Jap Fish Res Edu Agen 49:21–26

Arakawa KY (1990) Natural spat collecting in the Pacific oyster *Crassostrea gigas* (Thunberg). Mar Behav Physiol 17:95–128

Clarke B, Otto F, Stuart-Smith R, Harrington L (2022) Extreme weather impacts of climate change: an attribution perspective. Environ Res: Climate 1:012001

Dekshenieks MM, Hofmann EE, Klinck JM, Powell EN (1996) Modeling the vertical distribution of oyster larvae in response to environmental conditions. Mar Ecol Prog Ser 136:97–110

Dekshenieks MM, Hofmann EE, Klinck JM, Powell EN (1997) A modeling study of the effects of size-and depth-dependent predation on larval survival. J Plankton Res 19:1583–1598

Ding Y, Chan JCL (2005) The East Asian summer monsoon: an overview. Meteorol Atmos Phys 89:117–142

Fujii M, Hamanoue R, Bernardo LPC, Ono T and others (2023) Assessing impacts of coastal warming, acidification, and deoxygenation on Pacific oyster (*Crassostrea gigas*) farming: a case study in the Hinase Area, Okayama Prefecture and Shizugawa Bay, Miyagi Prefecture, Japan. Biogeosciences 20:4527–4549

Fujiya M (1970) Oyster farming in Japan. Helgoländer Wiss Meeresunters 20:464–479

Gamain P, Roméro-Ramirez A, Gonzalez P, Mazzella N, Gourves PY, Compan C, Cachot J (2020) Assessment of swimming behavior of the Pacific oyster D-larvae (*Crassostrea gigas*) following exposure to model pollutants. Environ Sci Pollut Res Int 27:3675–3685

Garland ED, Zimmer CA, Lentz SJ (2002) Larval distributions in inner-shelf waters: the roles of wind-driven cross-shelf currents and diel vertical migrations. Limnol Oceanogr 47:803–817

Hidu H, Haskin HH (1978) Swimming speeds of oyster larvae *Crassostrea virginica* in different salinities and temperatures. Estuaries 1:252–255

Hirata Y, Wakano M, Takayama K, Akashige S (2006) Growth and survival of oyster spat under environment of hardening process in Hiroshima Bay. Bull Hiroshima Pref Fish Mar Tech Cent 1:1–7 (in Japanese)

His E, Seaman MNL (1992) Effects of temporary starvation on the survival, and on subsequent feeding and growth, of oyster (*Crassostrea gigas*) larvae. Mar Biol 114:277–279

Hofmann EE, Powell EN, Bochenek EA, Klinck JM (2004) A modelling study of the influence of environment and food supply on survival of *Crassostrea gigas* larvae. ICES J Mar Sci 61:596–616

Kakehi S (2022) Developing short-term predictions for the distribution of Pacific oyster *Crassostrea gigas* larvae. Fish Sci 88:593–608

Kakehi S, Kamiyama T, Abe H, Hanawa S, Oota H, Matsuura R, Oshino A (2016) Mechanisms leading to the decline in Pacific oyster *Crassostrea gigas* seedlings in Matsushima Bay, Japan. Fish Sci 82:499–508

Kakehi S, Shirai H, Magome S, Takagi T and others (2020) Predicting the larval transport of Pacific oyster *Crassostrea gigas* during the seedling collection season. Fish Oceanogr 29:484–504

Kamiyama T, Yamauchi H, Iwai T, Hanawa S, Matsuyama Y, Arima S, Kotani Y (2005) Comparison of environmental conditions in two representative oyster farming areas: Hiroshima Bay, western Japan and Oginohama Bay (a branch of Ishinomaki Bay), northern Japan. Fish Sci 71: 1295–1303

Kennedy VS (1996) Biology of larvae and spat. In: Kennedy VS, Newell RI, Eble AF (eds) The eastern oyster: *Crassostrea virginica*. Maryland Sea Grant Publication, College Park, MD, p 371–421

Kikuchi S (1960) Considerations on the distributions of oyster larvae in Matsushima Bay. Bull Tohoku Nat Fish Res Inst 16:118–126 (in Japanese with English abstract)

Kimura T, Kaneyasu T, Hamamoto T (1975) Effect of the sea water movements forced by the wind on the decreasing of oyster larvae in the northern part of Hiroshima Bay. Aquat Sci 23:75–79 (in Japanese)

Koganezawa A (1978) Ecological study of the production of seeds of the Pacific oyster, *Crassostrea gigas.* Nihonkaiku Suisan Kenkyujo Kenkyu Hokoku 29:1–88 (in Japanese with English abstract)

Kunze HB, Morgan SG, Lwiza KM (2013) Field test of the behavioral regulation of larval transport. Mar Ecol Prog Ser 487:71–87

Kuroda H, Setou T, Kakehi S, Ito S and others (2017) Recent advances in Japanese fisheries science in the Kuroshio-Oyashio region through development of the FRA-ROMS ocean forecast system: overview of the reproducibility of reanalysis products. Open J Mar Sci 7:62–90

Kusuki Y (2009) Oyster farming in Hiroshima during the Showa Era. Kureseihan, Hiroshima (in Japanese)

Kusuki Y, Hirata S, Ouchi A, Aida S (1992) Distribution patterns of oyster larvae in Hiroshima Bay. 1. Change of distribution over a short period. Bull Hiroshima Fish Exp Stn 17:1–9 (in Japanese with English abstract)

Lagarde F, Ubertini M, Mortreux S, Bernard I and others (2017) Recruitment of the Pacific oyster *Crassostrea gigas* in a shellfish-exploited Mediterranean lagoon: discovery, driving factors and a favorable environmental window. Mar Ecol Prog Ser 578:1–17

Lagarde F, Fiandrino A, Ubertini M, d'Orbcastel ER and others (2019) Duality of trophic supply and hydrodynamic connectivity drives spatial patterns of Pacific oyster recruitment. Mar Ecol Prog Ser 632:81–100

Lee I, Fujita K, Takasugi Y, Hoshika A (2001) Numerical simulation of residual current and material transportation in Hiroshima Bay. Oceanogr Jpn 10:495–507 (in Japanese with English abstract)

Mann RL, Rainer JS (1990) Effect of decreasing oxygen tension of swimming rate of *Crassostrea virginica* (Gmelin, 1791) larvae. J Shellfish Res 9:323–327

Matsubara T, Yamaguchi M, Abe K, Onitsuka G and others (2023) Factors driving the settlement of Pacific oyster *Crassostrea gigas* larvae in Hiroshima Bay, Japan. Aquaculture 563:738911

McVeigh DM, Eggleston DB, Todd AC, Young CM, He R (2017) The influence of larval migration and dispersal depth on potential larval trajectories of a deep-sea bivalve. Deep Sea Res I 127:57–64

Mizuno K, Wakano M, Takatsuji H, Nagai T (2015) Effects of the dinoflagellate *Karenia mikimotoi* on larval settlement of Pacific oyster *Crassostrea gigas.* Bull Jpn Soc Sci Fish 81:811–816 (in Japanese with English abstract)

North EW, Hood RR, Chao SY, Sanford LP (2006) Using a random displacement model to simulate turbulent particle motion in a baroclinic frontal zone: a new implementation scheme and model performance tests. J Mar Syst 60:365–380

North EW, Schlag Z, Hood RR, Li M, Zhong L, Gross T, Kennedy VS (2008) Vertical swimming behavior influences the dispersal of simulated oyster larvae in a coupled particle-tracking and hydrodynamic model of Chesapeake Bay. Mar Ecol Prog Ser 359:99–115

Onduka T, Mizuno K, Shikata T, Mastubara T, Onitsuka G, Hamaguchi M (2022) Assessment of the risk posed by three antifouling biocides to Pacific oyster embryos and larvae in Hiroshima Bay, Japan. Environ Sci Pollut Res Int 29:9011–9022

Ono T, Muraoka D, Hayashi M, Yorifuji M and others (2024) Short-term variation of pH in seawaters around coastal areas of Japan: characteristics and forcings. Biogeosciences 21:177–199

Peteiro LG, Shanks AL (2015) Up and down or how to stay in the bay: retentive strategies of Olympia oyster larvae in a shallow estuary. Mar Ecol Prog Ser 530:103–117

Poulin E, Palma AT, Leiva G, Narvaez D, Pacheco R, Navarrete SA, Castilla JC (2002) Avoiding offshore transport of competent larvae during upwelling events: the case of the gastropod *Concholepas concholepas* in Central Chile. Limnol Oceanogr 47:1248–1255

Puckett BJ, Eggleston DB, Kerr PC, Luettich RA Jr (2014) Larval dispersal and population connectivity among a network of marine reserves. Fish Oceanogr 23:342–361

R Core Team (2021) R: a language and environment for statistical computing. R Foundation for Statistical Computing, Vienna. www.R-project.org/

Ray NE, Fulweiler RW (2021) Meta-analysis of oyster impacts on coastal biogeochemistry. Nat Sustain 4:261–269

Robins P, King J, Jenkins S, Tita A (2017) Predicting the dispersal of wild Pacific oysters *Crassostrea gigas* (Thunberg, 1793) from an existing frontier population — a numerical study. Aquat Invasions 12:117–131

Sugawara Y, Ishinomaki MJ, Oiwa M, Matsumoto Y and others (2000) Vertical distribution of oyster larvae. Bull Miyagi Pref Fish Res Dev Center 16:99–108 (in Japanese)

Suquet M, Rimond F, Cosson J, Wilson-Leedy J and others (2013) Effect of age and environmental conditions on the movement characteristics of Pacific oyster (*Crassostrea gigas*) trochophores. J Appl Ichthyology 29:1145–1148

Troost K, Veldhuizen R, Stamhuis EJ, Wolff WJ (2008) Can bivalve veligers escape feeding currents of adult bivalves? J Exp Mar Biol Ecol 358:185–196

Umehara A, Asaoka S, Fujii N, Otani S and others (2018) Biological productivity evaluation at lower trophic levels with intensive Pacific oyster farming of *Crassostrea gigas* in Hiroshima Bay, Japan. Aquaculture 495:311–319

Visser AW (1997) Using random walk models to simulate the vertical distribution of particles in a turbulent water column. Mar Ecol Prog Ser 158:275–281

Vogeler S, Bean TP, Lyons BP, Galloway TS (2016) Dynamics of nuclear receptor gene expression during Pacific oyster development. BMC Dev Biol 16:33

Wahyudin, Yamamoto T (2020) Modeling bottom-up and top-down controls on the low recruitment success of oyster larvae in Hiroshima Bay, Japan. Aquaculture 529:735564

Yamamoto H, Yamamoto T, Takada T, Mito Y, Takahashi T (2011) Dynamic analysis of oxygen-deficient water mass formed in the northern part of Hiroshima Bay using a pelagic-benthic coupled ecosystem model. Mizu Kankyo Gakkaishi 34:19–28 (in Japanese with English abstract)

Yamamoto T (2003) The Seto Inland Sea—eutrophic or oligotrophic? Mar Pollut Bull 47:37–42

Yamamoto T, Orimoto K, Asaoka S, Yamamoto H, Onodera SI (2021) A conflict between the legacy of eutrophication and cultural oligotrophication in Hiroshima Bay. Oceans (Basel) 2:546–565

Yamamoto T, Nakahara S, Hiraoka K, Fukuoka K (2023) Efficacy of the application of organic fertilizer to oyster growth. Mar Pollut Bull 187:114512

Editorial responsibility: Eric Sanford, Bodega Bay, California, USA
Reviewed by: 3 anonymous referees

Submitted: October 11, 2023
Accepted: June 4, 2024
Proofs received from author(s): July 16, 2024